A TRANS-EUROPEAN NETWORK OF CAMERAS FOR OBSERVATION OF NOCTILUCENT CLOUDS FROM 37°N TO 69°N

G. Baumgarten, M. Gerding, B. Kaifler, and N. Müller

Leibniz-Institut für Atmosphärenphysik (IAP), 18225 Kühlungsborn, Germany

ABSTRACT

A network of digital cameras was installed for online observation of noctilucent cloud (NLC) occurrence. One of the northernmost cameras allows to observe the NLC structure above ALOMAR (69°N,16°E) and the Esrange (68°N,21°E). During the ECOMA/MASS sounding rocket campaign in July/August 2007 the camera in Trondheim was used to identify good science conditions for the rocket launch. For real time investigation of the NLC presence the camera observations are transferred via Internet. The actual observations are available to the science community and public and allow to trigger detailed observations. For analysis of horizontal structure and a detailed comparison to lidar measurements at ALOMAR, Esrange and Kühlungsborn we have developed a high resolution ray-tracing algorithm. We have analyzed the camera observations from the years 2007 and 2008 and show the results for camera locations between 63°N and 43°N. During two seasons we have not observed a NLC from the southernmost camera at 37°N. We find that most NLC are observed between -5° and -17° solar elevation. Using these results we investigate the efficiency for the detection of the clouds throughout the season and the day. We observe that the daily mean detection efficiency at summer solstice is largest between 51°N and 54°N where NLC observations are possible throughout about 25% of the day. At southern latitudes of about 43°N the detection efficiency decreases to about 10%. Poleward of about 60° NLC can not be seen at solstice due to the high solar elevation. The solar elevation significantly affects the detection efficiency of NLC throughout the season. While the observations south of 55°N show a peak occurrence about 20 days after solstice, the observations at 63°N peak 40 to 50 days after solstice.

Key words: Noctilucent clouds; gravity waves; camera; network.

1. INTRODUCTION

Noctilucent clouds (NLC) are impressive optical phenomena with remarkable structures and temporal evolution. They have been observed from ground since 1885 but still their formation is not completely understood [e.g. 15]. The clouds are found at an altitude of about 83 km with small year to year variations of about 1 km only but a larger variation on short scales [12, 23, 7]. The clouds have attracted the interest of atmospheric physicists as their formation is a rather complicated process involving temperature, water vapor and condensation nuclei [22, 18]. It is speculated that a trend in the cloud occurrence is linked to global change, however the interpretation is more complicated [20, 21]. Extensive studies of noctilucent clouds by visual methods from ground were performed already at the end of the 19th century [11]. Since then several remote sensing methods from ground and space as well as in-situ methods have been developed to investigate the nature of the clouds. The different methods address different aspects of the clouds, most of them using sunlight scattered at the clouds [e.g. 10, 13, 5, 6]. Active sounding of these clouds by lidar have recently become available on a routine basis. As the different methods address different aspects of the clouds a combined analysis and a comparison of the different methods is still outstanding. We present the first results from our Trans-European NLC camera network and investigate the effect of the latitude dependence of solar illumination on the cloud observations. This network will allow a combined analysis using different instruments, e.g. lidar or satellite.

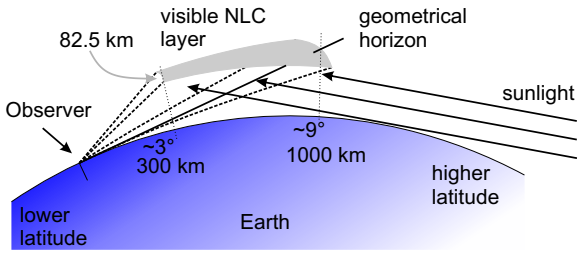

Figure 1. Noctilucent cloud observation geometry. The clouds become visible when the sun is below the horizon but still illuminating the clouds. If the upper cloud limit is observed at 12° elevation the cloud edge is located about 3° of latitude further north than the observer. Due to atmospheric refraction the clouds can be observed below the geometrical horizon.

Proc. '19th ESA Symposium on European Rocket and Balloon Programmes and Related Research, Bad Reichenhall, Germany, 7–11 June 2009 (ESA SP-671, September 2009)

2. INSTRUMENT AND METHOD

Table 1. Location and pointing of the IAP NLC cameras. Different camera types are used. The camera types are given for the years 2007/2008/2009. Type 0: Canon G3, type 1: Canon G6, type 2: Canon DSLR 450D. The field of view of the cameras is about 54° horizontally and 40.5° vertically for type 0 and 1. Type 2 has a field of view of about 49.7° × 34.3°.

Location	Lat.,Long. [°]	Az. , El. [°]	Type
ALOMAR (Andenes)	69.3, 16.0	10, 12	-/-/1
Lycksele	64.9, 18.8	0, 12	-/-/2
Trondheim	63.4, 10.4	22, 12	1/2/2
Juliusruh	54.6, 13.4	12, 14	1/1/1
Kühlungsborn	54.1, 11.8	22, 17	1/1/1
Katlenburg-Lindau	51.7, 10.2	-14, 15	0/0/1
Collm	51.3, 13.0	-14, 16	1/1/2
Pic du Midi	42.9, 0.1	35, 15	1/1/1
Calar Alto NW	37.2, -2.6	325, 15	-/-/2
Calar Alto NE	37.2, -2.6	35, 15	1/1/2

We have developed an automated camera system consisting of a high-resolution digital camera (7 to 15 Megapixels) and a computer to control the camera. During summer 2009 more than 10 cameras are in operation spanning a broad range of latitudes, namely from 37° N to 69° N (see Table 1). For the automated observation of the sky in the twilight period a control software was developed which allows the cameras to cover the huge dynamic range of the sky radiance. The camera system calculates the exposure settings and the frame rate automatically from the solar elevation. Starting from the tabulated exposure settings we modify the exposure settings according to the brightness of the last picture acquired. For each picture we calculate the histogram of brightnesses in the area of the twilight arch and make sure that there are no over- or under-exposed regions. Throughout the twilight period the cameras work continuously and deliver two to twenty pictures per minute. The cameras at latitudes between 51° N and 69° N look roughly towards north (or towards the lidar stations) as their FOV is large enough to observe sunset and sunrise. The lower latitude cameras at Pic du Midi (43° N), and Calar Alto NW (37° N) look only towards sunrise. At Calar Alto another camera was installed in spring 2009 looking to the dawn. The pictures are sent via Internet to the IAP on a near real-time basis and are stored into archives. During the NLC season the compressed data volume is about 7 GByte/day. The field of view (FOV) of the cameras is shown in Figure 2 where the shaded regions show the FOV of the cameras at NLC altitude projected to the ground.

For the interpretation of the images acquired by the cameras we map the pictures to a satellite view [16]. For an accurate projection of the cloud the pointing of the camera needs to be known precisely. The viewing geometry is calibrated using stars visible in the images. This alignment is performed shortly before or after special campaigns e.g. for the comparison to lidar observations. For the projection the corresponding azimuth and elevation of each point on the camera (pixel) is calculated. For each pixel we perform a ray-tracing taking the density profile at the given location from NRLMSISE-00 into account [17]. From the density we calculate the refractive index of the atmosphere via $n = \sqrt{(1 + b \cdot p)}$ where n is the refractive index, $b = 0.45211$/Pa and p is the pressure [14]. We apply the Snellius law of refraction assuming a layered atmosphere, depending on the elevation and the local pressure [e.g. 1]. In Table 2 we have summarized the results from the ray-tracing for the camera in Trondheim looking in direction of ALOMAR. Since the algorithm tracing the rays needs a lot of computer resources it is performed only after the camera FOV has changed. The ray-tracing results in a matrix for conversion of the source picture to the projected picture in spherical coordinates. Using the result matrix the projection of the images is quite fast and about two 12 MPixel pictures can be projected per second, while the ray-tracing takes about 15 minutes on a 3 GHz Xeon processor. Since the largest refraction occurs in the lower atmosphere we use a variable resolution depending on the density changes in the ray path. By this the ray-tracing is much faster when tracking the rays through the strato- and mesosphere. We apply the same ray-tracing results to the three color channels (red, green, blue) of the pictures. Table 2 shows that the atmospheric refraction modifies the location of the cloud by less than 100 m for elevations above 30°. At

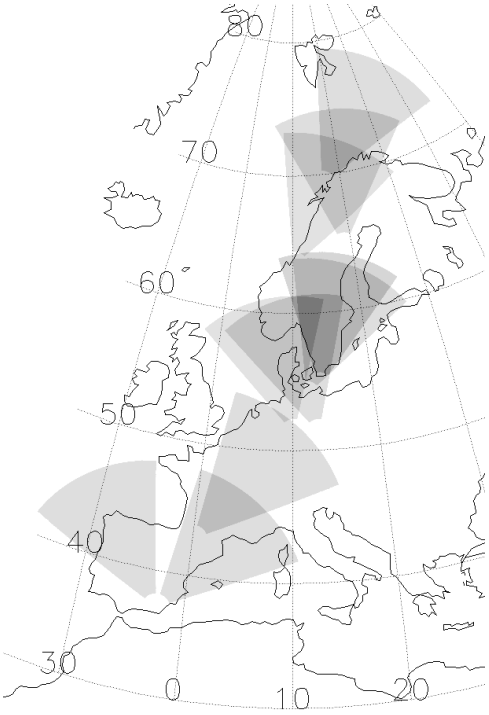

Figure 2. Overview of the IAP NLC camera network. Grey shaded areas show the field of view of each camera projected to the altitude of 83 km. The cameras can observe NLC from 38°N to nearly 80°N.

Table 2. Results of the ray-tracing algorithm for the NLC camera in Trondheim looking towards ALOMAR. For different elevation angles we have calculated the loci of the NLC observed under the assumption that the cloud altitude is z=83 km. Δrange is the range variation for 1 km cloud altitude change. ΔLatitude lists the effect of atmospheric refraction on the beam propagation. AOI is the angle of incidence at the NLC layer. The brightness factor gives the increase of the apparent NLC brightness due to a longer volume throughout a homogeneous NLC layer, depending on the AOI.

Elevation [°]	Latitude [°]	Longitude [°]	Range [km]	ΔRange [km]	ΔLatitude [10^{-3} °]	ΔLatitude [km]	AOI [°]	Brightness Factor 1
0	72.36	19.63	1074	6.3	342.8	42.22	9.1	6.32
1	71.43	18.25	961	6.2	277.6	33.85	9.1	6.32
2	70.58	17.10	857	6.4	195.8	23.68	9.3	6.19
3	69.83	16.18	768	5.9	138.4	16.62	9.6	6.00
4	69.20	15.44	691	5.7	99.7	11.91	9.9	5.82
5	68.64	14.84	625	5.6	73.7	8.75	10.4	5.54
6	68.17	14.35	569	5.3	55.2	6.53	10.9	5.29
7	67.75	13.94	520	5.0	42.3	4.98	11.5	5.02
8	67.39	13.59	477	5.0	32.1	3.76	12.1	4.77
9	67.08	13.30	440	4.5	21.1	2.44	12.8	4.51
10	66.81	13.05	409	4.3	20.6	2.39	13.5	4.28
12	66.35	12.65	356	3.9	14.5	1.67	15.0	3.86
14	65.99	12.35	314	3.5	9.2	1.05	16.6	3.50
16	65.70	12.11	281	3.2	6.6	0.74	18.3	3.18
18	65.46	11.91	254	2.9	4.2	0.45	20.1	2.91
20	65.26	11.75	232	2.7	3.7	0.41	21.9	2.68
25	64.88	11.46	191	2.3	2.1	0.22	26.5	2.24
30	64.61	11.26	163	1.9	1.2	0.12	31.2	1.93
35	64.40	11.10	143	1.7	0.7	0.07	36.0	1.70
40	64.24	10.99	128	1.5	0.5	0.04	40.8	1.53
50	64.00	10.81	108	1.3	0.3	0.02	50.6	1.29
60	63.82	10.68	96	1.1	0.1	0.01	60.4	1.15
70	63.67	10.58	88	1.1	0.1	0.00	70.3	1.06
80	63.54	10.49	84	1.0	0.0	0.00	80.1	1.02
90	63.41	10.40	83	1.0	0.0	0.00	90.0	1.00

the horizon the refraction leads to a dislocation of about 40 km when neglecting the atmospheric refraction. We realize that the clouds are about 1100 km away when observed at the horizon. Since the brightness of NLC depends (amongst others) on the path length through the clouds we have calculated the geometrical aspects of the path length. As the path length through the clouds can be calculated from the angle between the ray and the NLC layer we have calculated the angle of incidence (AOI) at the layer. The NLC brightness at low elevation angles is increasing proportional to the column factor which is calculated via $1/\sin(\text{AOI})$. Please note that also the angular dependence of the scattering on NLC particles enhances the NLC brightness at low elevations. At low elevations the scattering is more forward directed which is pronounced on the nanometer-sized NLC particles [3].

2.1. Improved setup for high resolution imaging

The camera setup was improved in spring 2009 to increase the resolution and to decrease the noise. The new camera Canon EOS 450D (sensor area = 3.28 cm^2) has a nearly 10 times larger chip area than the G6 (sensor area = 0.38 cm^2) and can therefore collect more light than the G6 when using a lens with the same f-number. Also the resolution of the cameras was increased from 7 to 12 MPixel for two reasons: (1) To maintain a large field of view of about 50° and (2) to increase the resolution of cloud structures. The EOS 450D is combined with a f=24 mm f/1.8 lens. This gives a resolution of about 40 m at 200 km distance which are reached at an elevation of about 25° (c.f. Table 2). To make use of the high resolution the exposure time has to be less than one second as the horizontal drift due to the wind-speed of about 40 m/s [19] at the cloud altitude would blur the structures in the cloud . For bright NLC displays, mostly from our camera at 63° N, we have observed exposure times of less than one second. For elevations above 25° the resolution is even higher, but this requires a bright NLC display which occurs less often. Studies on scales shorter than 40 m require a lens with a larger focal length but maintaining the f-number of about f/2. By this the resolution is increased while maintaining the same exposure times. For example combining a 15 MPixel camera (EOS 50D) with a f=135 mm lens gives a resolution of about 7 m at an elevation of 25° or less than 5 m at elevations above 45°. For this high resolutions the exposure time needs to be less than 1/10 second to minimize blurring of the

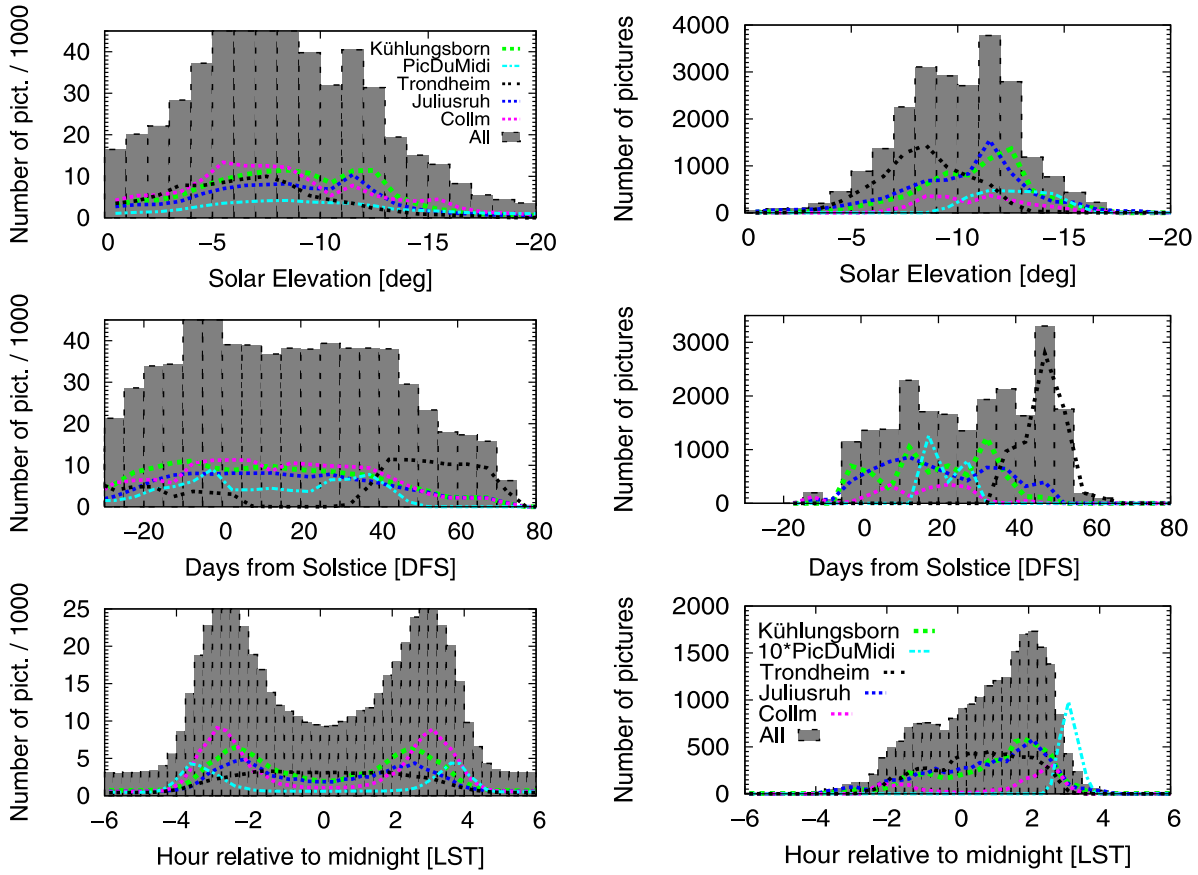

*Figure 3. Pictures of all NLC cameras acquired during summer 2007 and 2008 (***left:** *with and without NLC, right: NLC only).*
Top: *Number of pictures against solar elevation angle.* **Middle:** *Number of pictures throughout the season.*
Bottom: *Number of pictures against local solar time. Please note that the number of pictures with NLC signatures at Pic du Midi was rescaled by a factor of 10.*

structures. Longer focal lengths require shorter exposure times to minimize the motion blurring, but this requires a higher gain on the sensor which results in higher noise.

3. OBSERVATIONS

The IAP NLC camera network covers the latitudes from 63°N to 37°N. In the summers 2007 and 2008 the camera network has acquired about 750000 camera pictures. To extend the lifetime of the cameras we have modified the frame rate depending on solar elevation and throughout the season. In the left column of Figure 3 we show the number of pictures throughout the day and the season. At solar elevation angles below -12°the frame rate decreases also due to the longer exposure times needed to collect enough light from the clouds. For the G6 cameras the maximum exposure time is 15 s while it can be up to 30 s plus 30 s dark-field compensation for the EOS 450D. In summer 2007 we have already reduced the frame rate end of July (Days from solstice (DFS)=40), while in summer 2008 we have extended the observations to DFS=60. Please note that the number of pictures per day also depend on the duration of the sunrise/set. We address this topic later in the manuscript.

We found NLC structures in about 24000 pictures in the period May 1 to August 30 by manual inspection of the observations. The observations are summarized in the right column of Figure 3. The upper right panel in Figure 3 shows the number of oservations as function of solar elevation. Most of the NLC pictures are taken between 0°and -17°. In the summers 2007 and 2008 we have observed the earliest NLC on DFS=-20 (June 1) with our camera in Juliusruh. The latest NLC was observed on DFS=64 (August 24) with our camera in Trondheim. The southernmost observations of NLC were performed with our camera at Pic du Midi (43° N) around DFS=20. As the number of pictures acquired depends on the frame rate we have calculated the NLC occurrence rate from our observation by dividing the number of NLC pictures by the total number of pictures binned in the same way (solar elevation in 1 ° steps, DFS in 5 day steps, LST in 15 min steps). In the left column of Figure 4 we show the NLC occurrence rate for the period DFS=0–50 to investigate the peak of the season. The result combining all NLC cameras shows a high chance of observing NLC between -5°and -17°solar elevation. The peak occurrence rate is

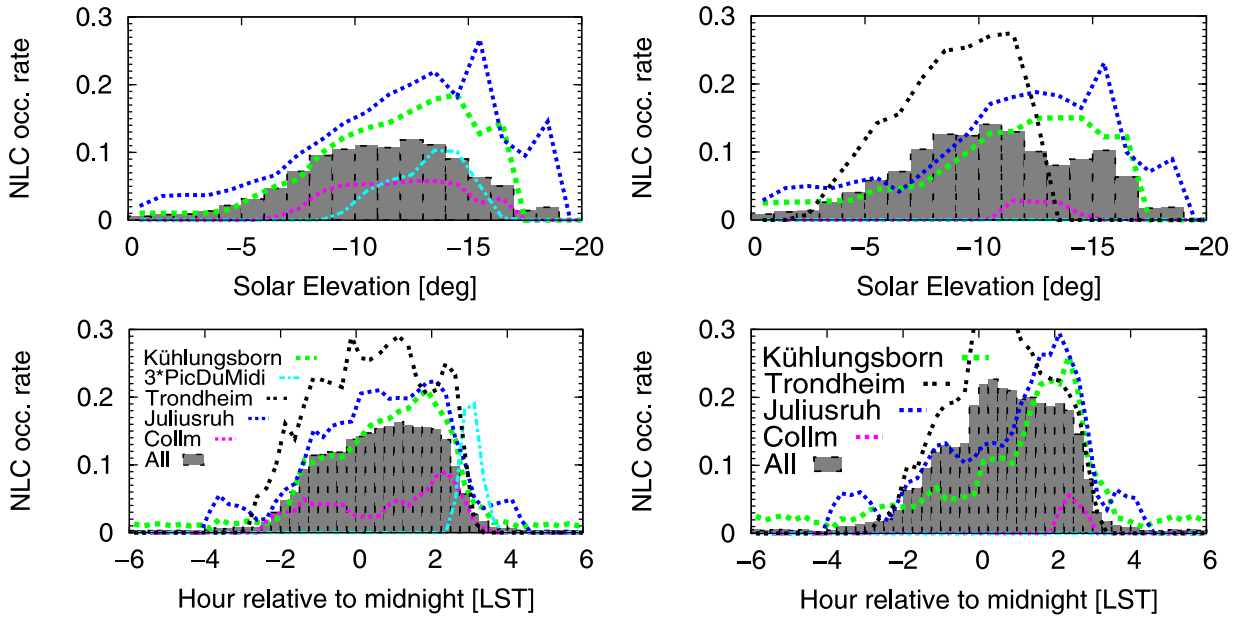

*Figure 4. Mean NLC occurrence frequency for the peak of the NLC season (***left:** *DFS=0–50) and the late NLC season (***right:** *DFS=30–60) during summer 2007 and 2008.*
Top: *Occurrence frequency observations against solar elevation angle.*
Bottom: *Occurrence frequency as function of local solar time. Please note that the observations at Pic du Midi were rescaled by a factor of three.*

about 10% between -8°and -14°solar elevation. This observation is in agreement to previous studies relying on experienced NLC observers [10]. Previous publications have reported the NLC observation period to fall between -6°and -16°solar elevation angle [9]. The slightly extended observation period of the cameras has probably two reasons: (1) for low solar elevations the long exposure of the camera and the high gain of the cameras lead to a higher low-light sensitivity. (2) For higher solar elevation angles the time-lapse of coherently moving NLC structures allows to detect NLC even during low contrast conditions (high background due to molecular scattering). The good agreement proves that the automated cameras are well capable of detecting even weak NLC structures. The median of the distribution is about -12°. We note that the peak solar elevation depends only slightly on the camera location. While it is -10°for 64°N (Trondheim) it is about -15°to -14°for 55° N and 54° N (Juliusruh/Kühlungsborn). At 43° N the clouds were observed most often between -12°– -14°solar elevation. This might be an indication of the clouds brightness or structures depending on latitude. Bright and structured clouds can be detected even at higher solar elevation angles while the detection of weak or less structured clouds requires a darker background.

4. DISCUSSION AND CONCLUSION

The NLC observations by camera show an extremely strong dependence on the solar elevation angle and hence on the local time. This is not in agreement with other instruments and is due to the solar illumination affecting the observations [e.g. 8]. Also from the observation geometry it is clear that only during a range of solar elevation angles the clouds are visible (c.f. Figure 1). We have investigated the effect of solar elevation on cloud detection in detail as shown in Figure 5. The upper panel of Figure 5 shows the minimum solar elevation angle at several camera locations throughout the season. One can see that the northernmost camera location allows NLC detection only from DFS=50 onwards. For the cameras at Lycksele or Trondheim the clouds become visible at DFS=30 (July 21) and DFS=20 (July 11), respectively.

To quantify the correct illumination conditions we calculate the NLC visibility as the ratio of the time that solar elevation is between -5°and -17°to the total time (either per day or per hour). The middle panel shows that the NLC visibility is highest for the cameras between 51°N and 59°N. The mean visibility between DFS=-20 and DFS=20 is about 27% per day. At the southernmost cameras the NLC visibility is more or less constant throughout the season but is only 10 – 12%. So only through 2.4 – 2.9 hours per day the illumination allows the detection of NLC. At these southern locations NLC are only visible about 4 hours before or after midnight. The observed diurnal variation of the NLC occurrence rate is largely influenced by the solar illumination. Nevertheless we observe that the NLC occurrence is higher in the morning hours than before midnight (c.f. Figure 4). This is in agreement with other observations [e.g. 8]. Furthermore we observe that the NLC occurrence decreases with latitude. For example from 55°N to 51°N the occurrence

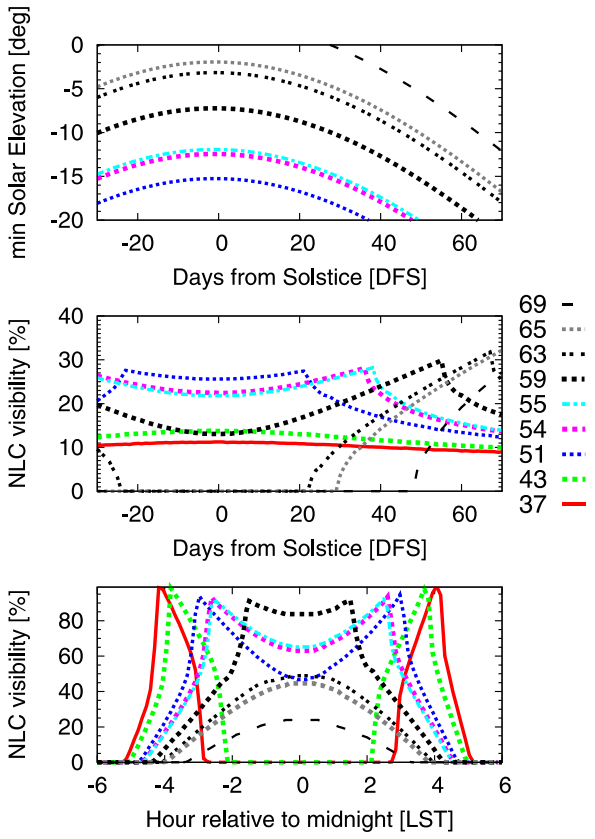

Figure 5. NLC visibility for the different camera locations (eg. 43: Pic Du Midi; 54: Kühlungsborn; 63: Trondheim) as deduced from the solar elevation angle. Due to the illumination conditions NLC become visible when the solar elevation is between -5°and -17°. **Top:** *Minimum solar elevation angle for the different camera locations* **Middle:** *NLC visibility throughout the season.* **Bottom:** *Seasonal average NLC visibility throughout the day (averaged only for days with sol. elevation below -5°).*

decreases from more than 25% to less than 5% and less than 4% at 43°N. This decrease is even stronger at the end of the season where we observe no NLC at 43°N at all.

For the analysis presented here we have not taken the weather conditions into account as this is not automated yet. We plan to implement an automatic clear sky and NLC detection by splitting the images into 8×8 sub images. In these images we calculate the brightness and the color ratios (red/green and blue/green) and their variances. We expect to find usefull thresholds to identify the clear sky and NLC. Furthermore we want to compare the observations in detail to lidar observations and extend previous studies [e.g. 2, 4].

ACKNOWLEDGMENTS

We are indebted to Michael Priester for supporting our project through installation and maintenance of the camera systems. We also like to thank several institutions which support our project by sharing their infrastructure at the various sites of our cameras.

REFERENCES

[1] Baumgarten, G. 2001, PhD thesis, Universität Bonn, BONN-IR-2001-10, Bonn, Germany

[2] Baumgarten, G., Fiedler, J., Fricke, K. H., et al. 2009, Annales Geophysicae, 27, 953

[3] Baumgarten, G., Fiedler, J., Lübken, F.-J., & von Cossart, G. 2008, J. Geophys. Res., 113, D06203

[4] Collins, R. L., Taylor, M. J., Nielsen, K., et al. 2009, Journal of Atmospheric and Solar-Terrestrial Physics, 71, 446

[5] Dalin, P., Pertsev, N., Zadorozhny, A., et al. 2008, Journal of Atmospheric and Solar-Terrestrial Physics, 70, 1460

[6] DeLand, M. T., Shettle, E. P., Thomas, G. E., & Olivero, J. J. 2006, J. Atmos. Sol.-Terr. Phys., 68, 9

[7] Fiedler, J., Baumgarten, G., & Lübken, F.-J. 2009, Journal of Atmospheric and Solar-Terrestrial Physics, 71, 424

[8] Fiedler, J., Baumgarten, G., & von Cossart, G. 2005, Ann. Geophys., 23, 1175

[9] Fogle, B. & Haurwitz, B. 1966, Space Science Reviews, 6, 279

[10] Gadsden, M. & Schröder, W. 1989, Noctilucent clouds (New York: Springer-Verlag)

[11] Jesse, O. 1889, Nature, 39, 537

[12] Jesse, O. 1896, Astron. Nachrichten, 140, 161

[13] Kirkwood, S., Barabash, V., Brändström, B. U. E., et al. 2002, Geophys. Res. Lett., 29, 1411

[14] Kneubühl, F. K. 1990, Repetitorium der Physik, B. G. Teubner (Stuttgart)

[15] Leslie, R. C. 1885, Nature (London), 32, 245

[16] Pautet, D. & Moreels, G. 2002, Appl. Optics, 41, 823

[17] Picone, J. M., Hedin, A. E., Drob, D. P., & Aikin, A. C. 2002, Journal of Geophysical Research (Space Physics), 107, 1468

[18] Rapp, M. & Thomas, G. E. 2006, J. Atmos. Sol.-Terr. Phys., 68, 715

[19] Singer, W., Latteck, R., Hoffmann, P., et al. 2005, Geophys. Res. Lett., 32

[20] Thomas, G. E., Olivero, J. J., Jensen, E. J., Schroeder, W., & Toon, O. B. 1989, Nature, 338, 490

[21] von Zahn, U. 2003, EOS Transactions, 84, 261

[22] Wegener, A. 1912, Gerlands Beitr. Geophysik, 11, 104

[23] Witt, G. 1962, Tellus, 14, 1